

Calibration of the Liverpool Telescope RINGO3 polarimeter

Aga Słowikowska¹, Krzysztof Krzeszowski¹, Michał Żejmo¹, Pablo Reig^{2,3}
and Iain Steele⁴

¹ *Janusz Gil Institute of Astronomy, University of Zielona Góra, Lubuska 2, 65-265 Zielona Góra, Poland*

² *Foundation for Research and Technology, 71110 Heraklion, Crete, Greece*

³ *University of Crete, Physics Department, PO Box 2208, 710 03 Heraklion, Crete, Greece*

⁴ *Astrophysics Research Institute, Liverpool John Moores University, L3 5RF, UK*

Released 2014

ABSTRACT

We present an analysis of polarimetric observations of standard stars performed over the period of more than three years with the RINGO3 polarimeter mounted on the Liverpool Telescope. The main objective was to determine the instrumental polarisation of the RINGO3 polarimeter in three spectral energy ranges: blue (350–640 nm), green (650–760 nm) and red (770–1000 nm). The observations were conducted between 2012 and 2016. The total time span of 1126 days was split into five epochs due to the hardware changes to the observing system. Our results should be applied to calibrate all polarimetric observations performed with the RINGO3 polarimeter.

Key words: polarimetry – polarisation standard stars – zero-polarised stars – polarised stars – polarisation calibration – RINGO3 polarimeter

1 INTRODUCTION

Polarimetry is an essential complement to photometric and spectroscopic studies because it provides additional constraints on existing theoretical models describing the physical processes standing behind emission of radiation. Radiation from astrophysical sources as a rule shows some degree of polarisation. However, the polarised radiation is often only a small fraction of the total radiation, with typical value of polarisation degree of a few percent. Polarised radiation carries a wealth of information on the physical state and geometry of the emitting source and interacting interstellar medium. Therefore, polarimetry often yields information that other methods of observations can not provide. Diagnostics of various astrophysical emission and radiation transfer phenomena are often based on polarimetric measurements. Good examples include optical polarimetric measurements simultaneous with gamma-ray flares in the blazar 3C279 (Abdo et al. 2010), polarimetry of optical afterglow of gamma ray bursts (e.g. GRB 120308A, Mundell et al. 2013), dust grains in the debris disk of AU Microscopii (Graham et al. 2007), polarised light from atmospheres of the solar planets and in extreme cases of exoplanets (e.g. Hansen & Hovenier 1974). High time resolution polarimetry is also important, for example in the case of fast rotating neutron stars such as the Crab pulsar (Słowikowska et al. 2009). An example of highly spatial resolution polarimetric observations of nebulae including highly polarised rotation powered pulsar nebulae such as the Crab nebula is presented by Moran et al. (2013).

A polarimeter measures the state of polarisation, or some aspects of the state of polarisation, of a beam of radiation. Ideally,

the values of all four Stokes parameters should be determinable, together with their variations with time, space, and wavelength. In practise, this is rarely possible, at least for astronomical sources. Most of the time only the degree of linear polarisation and its direction are found. There is a variety of the polarimetry measurement techniques. They range from the simplest one, i.e. looking through a polariser or the equivalent at other wavelengths, to specialised use of time varying wave plates and detectors like CCDs or radio interferometry arrays. The precise form of the instrument depends on the wavelength range for which it is designed.

Proper polarimeter calibration is the most critical issue for all polarimetric measurements in order to get reliable results. It is achieved with long term monitoring of polarised and zero-polarised standard stars. Observations of both types of standard stars are required to determine instrumental polarisation and depolarisation. Calibration is a necessary step to be able to compare measurements taken with different instruments or the same instrument at different epochs.

In this paper we present our data analysis of a number of polarised and zero-polarised standard stars obtained with the RINGO3 polarimeter mounted on the Liverpool Telescope - the biggest optical, fully robotic telescope on the world, as a function of time with the aim of providing useful information for other users of the instrument. We describe the three colour RINGO3¹ polarimeter in Sec. 2. The observations are described in Sec. 3 while the data analysis is described in Sec. 4. We present our results in Sec. 5

¹ <http://telescope.livjm.ac.uk/TelInst/Inst/RINGO3/>

and summarise our work in Sec. 6, whereas in the Appendix we present some of the details of our calculations, figures showing the normalized Stokes parameters, PD and PA as a function of time for BD +59 389, BD +64 106, G 191 B2B and HD 14069. Additionally, we also give there the tables with the coefficients of linear fits to the normalized Stokes q and u parameters for two zero-polarized standard stars.

2 RINGO3 POLARIMETER

RINGO3 (Arnold et al. 2012) is a fast-readout optical imaging polarimeter at the Liverpool Telescope (Steele et al. 2004). Unlike the original RINGO² which used deviating optics to spread the time varying polarised signal into rings, RINGO3 uses a fast readout camera to capture this signal as it changes in time. It is fed by a 45 degree folding mirror from the telescope main beam. The first optical element in the system is a field lens that places the telescope pupil close to the position of the dichroic mirrors farther down the optical path. This serves to reduce the vignetting in the instrument. Following this is a high quality wire grid polariser that rotates approximately once per second. It is this time varying signal that the instrument records in order to measure the polarisation of light entering the instrument. Following the rotating polariser, a collimator lens is used to collimate the beam. A pair of dichroic mirrors then splits the beam into three for simultaneous polarised imaging in three wavebands with separate camera lens and detector systems with approximate wavelength ranges of: blue 350–640 nm, green 650–760 nm and red 770–1000 nm. The colours of the RINGO3 cameras therefore approximately correspond to the B+V, R and I Johnson filters respectively. Each camera receives eight exposures per polariser rotation. These exposures are electronically synchronised with the phase of the polariser’s rotation. Therefore in a typical one minute exposure the instrument will produce ~ 60 frames at each phase (i.e. a total of ~ 480 frames). All frames for each matched phase are then stacked to obtain a single image at each phase of the polariser’s rotation for the purposes of data analysis.

The detectors comprise a 512×512 pixel electron multiplying CCD (EMCCD) cameras with negligible dark current. These yield a field of view of $\sim 4 - 5$ arcmin diameter. The field of view and pixel scale varies slightly for each camera due to their slightly different optical arrangements. Tests on the highly polarised twilight sky show that there is no significant dependence of measured polarisation with position in the unvignetted field.

The EMCCD gain can be set to values of 5, 20 or 100. For sources fainter than $V \sim 10$ a gain of 100 is used. For brighter sources a gain of 20 is generally employed. An EMGAIN of 100 corresponds to a gain value of around 0.32 electrons/ADU in a single ~ 125 -ms frame. As described above the data pipeline automatically stacks images to create a mean frame from a given polaroid phase. Therefore, the final gain of an image can be calculated by multiplying 0.32 by the number of frames that were stacked.

For proper data calibration two types of polarimetric standard stars need to be observed. By default polarised as well as zero-polarised standard stars are observed robotically each night. The zero-polarised standard stars allow correction of the instrumental polarisation, while the polarised standard stars correct for the instrumental depolarisation. The Liverpool Telescope has an altitude-azimuth mount with associated Cassegrain rotator. To minimise a

potential source of systematic error these standard star observations are obtained at the same rotator mount position angle as the science data. In general the mount position angle of zero is used for all RINGO3 observations (science and standard stars). To calculate the true sky position angle it is necessary to take into account the sky position angle and the mechanical mount position. Both values are stored in the FITS files headers as *ROTSKYPA* and *ROTANGLE*, respectively.

3 OBSERVATIONS

Both zero and polarised standard stars have been and are regularly scheduled and observed during most nights with RINGO3. In this paper we analyse data from 2012, December 7th (56268 MJD) until 2016, January 7th (57394 MJD), i.e. throughout whole RINGO3 life cycle after the commissioning. The data were obtained from the public archive available on the LT web page³. Within that time span there were four hardware changes, one of which also coincided with the re-aluminisation of the telescope’s primary and secondary mirrors, i.e.:

2013-01-23 (56315 MJD) On this date the field lens was changed to optimise the vignetting. In the process of doing this the polariser was rotated relative to the electronic synchronisation reference sensor.

2013-12-12 (56638 MJD) On this date a Lyot depolariser (DPU-25 Quartz-Wedge Achromatic Depolariser, uncoated 190–2500 nm, Thorlabs) was installed between the rotating polariser and the collimator lens to address the issues identified in Sec. 5 below where an interaction between the rotating polarised beam output by the polariser and the dichroic mirror coatings is identified. By depolarising the beam after the polariser (since at that stage we are only interested in measuring its time variable intensity) we reduce this interaction.

2014-06-08 (56816 MJD) On this date the depolariser was moved from the input to the output of the collimator. By moving it to the collimated beam, its depolarisation efficiency was increased since in a Lyot type depolariser the depolarisation obtained is related to the incident beam width.

2015-06-27 (57200 MJD) On this date the re-aluminisation of the primary and secondary mirrors was undertaken. The mirror recoating gave a large (factor ~ 2) throughput increase. Additionally, the polariser rotation was slowed down from one revolution per second to ~ 0.4 rotations per second with the change of motor gearbox ratio. This was done in order to improve signal-to-noise ratio for faint targets. A side effect of this change was that the direction of rotation was reversed. This caused the numerical sign of the Stokes $u=U/I$ parameter to flip compared with data taken before this date.

Hardware changes to the system introduced instrumental polarisation and depolarisation. Therefore we decided to split all the data within respect to the dates of four hardware changes into five epochs. The knowledge of the system calibration in each of the epochs is required in terms of proper data analysis. Information about standard stars used in our analysis are gathered in Table 1 and Table 2 (Turnshek et al. 1990; Schmidt et al. 1992), regarding their photometric as well as polarimetric characteristics, respectively.

All three detectors of RINGO3 are the EMCCD. The EMGAIN setting affects SNR in such a way that a lower EMGAIN

² <http://telescope.livjm.ac.uk/TelInst/Inst/RINGO/>

³ http://telescope.livjm.ac.uk/cgi-bin/lt_search

Table 1. Polarisation coordinates of standard stars, brightness and spectral types. Data analysis of four first listed standard stars is presented in Sec. 4, while the results for all nine standard stars based on the data obtained during the last (fifth) epoch are given in Sec. 6.

Name	RA	Dec	B	V	R	I	Spec. Type	Comments
BD +59 389	02 02 42.09	+60 15 26.46	10.03	9.08	8.49	8.23	F0Ib	—
BD +64 106	00 57 36.71	+64 51 26.50	10.87	10.29	9.90	9.84	B1	—
G 191-B2B	05 05 30.61	+52 49 51.96	11.43	11.67	11.82	11.45	DA.8	White Dwarf
HD 14069	02 16 45.19	+07 41 10.67	9.21	9.06	8.97	8.91	A0	—
BD +25 727	04 44 24.92	+25 31 42.72	10.20	9.55	9.11	8.98	A2 III	—
HD 155528	17 12 19.95	-04 24 09.26	10.05	9.61	9.32	9.16	B9	—
HD 215806	22 46 40.24	+58 17 43.94	9.55	9.21	8.99	—	B0Ib	—
HILT 960	20 23 28.53	+39 20 59.05	11.45	10.46	9.84	9.49	B0V	—
VI CYG 12	20 32 40.96	+41 14 29.29	14.45	11.78	11.96	8.41	B3-4 Ia+	—

Table 2. Summary of the archival polarimetric measurements of standard stars, ref: H - *The Hubble Space Telescope Northern-Hemisphere grid of stellar polarimetric standard stars* (Schmidt et al. 1992), S - *Systematic variations in the wavelength dependence of interstellar linear polarisation* (Whittet et al. 1992).

Name	Johnson filter	PD [%]	PA [°]	ref
BD +59 389	B	6.345 ± 0.035	98.14 ± 0.16	H
	V	6.701 ± 0.015	98.09 ± 0.07	H
	R	6.430 ± 0.022	98.14 ± 0.10	H
	I	5.797 ± 0.023	98.26 ± 0.11	H
BD +64 106	B	5.506 ± 0.090	97.15 ± 0.47	H
	V	5.687 ± 0.037	96.63 ± 0.18	H
	R	5.150 ± 0.098	96.74 ± 0.54	H
G 191-B2B	I	4.696 ± 0.052	96.89 ± 0.32	H
	B	0.090 ± 0.048	—	H
HD 14069	V	0.061 ± 0.038	—	H
	B	0.111 ± 0.036	—	H
BD +25 727	V	0.022 ± 0.019	—	H
	B	5.930 ± 0.070	31.00 ± 1.00	S
BD +25 727	V	6.290 ± 0.050	32.00 ± 1.00	S
	R	6.290 ± 0.070	31.00 ± 1.00	S
	I	5.680 ± 0.070	31.00 ± 1.00	S
	B	4.612 ± 0.038	91.24 ± 0.24	H
HD 155528	V	4.986 ± 0.064	92.61 ± 0.37	H
	R	—	—	-
	I	—	—	-
HD 215806	B	1.870 ± 0.040	66.00 ± 1.00	S
	V	1.840 ± 0.050	67.00 ± 1.00	S
	R	1.830 ± 0.040	66.00 ± 1.00	S
	I	1.530 ± 0.050	67.00 ± 1.00	S
HILT 960	B	5.720 ± 0.061	55.06 ± 0.31	H
	V	5.663 ± 0.021	54.79 ± 0.11	H
	R	5.210 ± 0.029	54.54 ± 0.16	H
VI CYG 12	I	4.455 ± 0.030	53.96 ± 0.19	H
	B	9.670 ± 0.100	119.00 ± 1.00	S
	V	8.947 ± 0.088	115.03 ± 0.28	H
VI CYG 12	R	7.893 ± 0.037	116.23 ± 0.14	H
	I	7.060 ± 0.050	117.00 ± 1.00	S

means a higher read noise and so worse SNR. During the observations the EMGAIN was set to 100 for the whole time for BD +64 106 and G 191-B2B, whereas for BD +59 389 as well as for HD 14069 the gain was set to 100 before 57200 MJD and was changed to 20 after this date, because both stars are brighter than 10th magnitude. However for such bright standards, the read noise is not really important.

4 DATA ANALYSIS

Data analysis was conducted in the following order: data gathering, image stacking, measuring flux, Stokes parameters calculations, PD and PA derivation with appropriate polarimetric corrections. Each step of analysis is described in detail below.

Firstly, we downloaded over 100,000 data frames from the public archive, including 73,552 frames for polarised sources (9,888 for BD +59 389; 10,536 for BD +64 106; 14,872 for BD +25 727; 17,280 for VI Cyg 12; 17,304 for Hilt 960; 1,440 for CRL 2688; 1,080 for HD 155528; 1,152 for HD 215806) and 30,672 frames for zero polarised sources (21,352 for G 191-B2B and 9,320 for HD 14069). Data analysis as well as the results of CRL 2688 are the topic of separated study, because it is extended source and not the point source as all the other targets. For the first part of the data analysis (Sec. 4 and Sec. 5) we concentrated only on four sources, two polarised ones, i.e. BD +59 389 and BD +64 106, and two zero-polarised, i.e. G 191-B2B and HD 14069. However, all sources listed in Table 1 were used for the summary and conclusions (Sec. 6) and their results are presented in Table 8 as well as in Fig. 10.

The data were debiased, flat fielded and had a World Coordinate System (WCS) fitted by the standard pipeline running at the telescope. Using the WCS coordinates we identified our targets and with the Source-Extractor (Bertin & Arnouts 1996) we extracted the target flux and its corresponding error with the best aperture. Thus, our input data consist of the flux value, its error as well as an information at which rotation angle (one of 0° , 45° , 90° , 135° , 180° , 225° , 270° , and 315°) this value was measured. Counting that the single set of observation consists of 8-frames there were 1236, 1317, 2669 and 1165 polarimetric measurements for BD +59 389 and BD +64 106, G 191-B2B and HD 14069, respectively. We selected only such observations for which all 8 flux values were available after the basic data reduction. This constrain removed 43, 50, 221 and 163 data points from sets of 8-frames for BD +59 389 and BD +64 106, G 191-B2B and HD 14069, respectively. Additionally, we applied the constraint on the PD error lower than 1% to data of all sources and the PD of G 191-B2B to be lower than 3%. We also filtered out the observations with seeing greater than 5 arc-sec. These conditions additionally removed the following number of data points for each source: 12 points from BD +59 389 data, 21 points from BD +64 106 data, 121 points from G 191-B2B data and 19 points from HD 14069 data. As a result we obtained a total of 5737 polarimetric measurements, i.e. 1181, 1246, 2327 and 983 for BD +59 389, BD +64 106, G 191-B2B and HD 14069, respectively.

To calculate the Stokes I, Q, and U we used method described by Sparks & Axon (1999) for n-polarisers. This method was very

successfully used before. One of the most extreme cases of using the n-polarisers method is the case of the Crab pulsar presented by Słowikowska et al. (2009) where measurements through as many as 180 positions of the rotating polariser were used to calculate PA and PD as a function of rotational phase of the neutron star. Regarding stellar optical polarimetry (apart from the Sun) this results gave the highest time resolution so far achieved, i.e. the polarisation was measured in the time scales down to ten microseconds. The greatest advantage of using more than three polarisers is the significant reduction of the errors of PD and PA.

For each source we calculated normalised Stokes parameters $q=Q/I$ and $u=U/I$ for data acquired from all three cameras. Because the RINGO3 hardware was changed multiple times (see Sec. 3) during the time span that covers our whole data set, we had to split the data into five parts and analyse them separately to remove the influence of the system changes. The resulting q-u diagrams are shown in Figs. A1, A4, A7 and A9 for BD +59 389, BD +64 106, G 191-B2B and HD 14069, respectively. Each q-u diagram consists of 15 panels. There are three rows corresponding to three camera colours (blue, green and red from the top to the bottom) and five columns for five MJD epochs. For polarised sources the q-u diagrams show points aligned in circular shape. This is caused by the fact that the LT telescope has an alt-az mount, therefore the data need to be corrected for the sky position angle of the image, i.e. how the rotation of the image relates to the North (see Eq. 2). The radius of the circle corresponds to the measured PD. Significant instrumental polarisation causes the centres of the circles to be shifted away from the zero-zero point. The same behaviour is visible in the q-u diagrams of zero-polarised stars. However, in such cases, instead of circles the data points form clumps. In order to remove the instrumental polarisation one needs to shift the data points to zero-zero origin. In case of polarised standard stars we fit the circles to the data points to get the coordinates of the circles centres, while in case of zero-polarised sources we calculated the weighted means in both directions (q, u) and treated these as the centres of the clumps. These way we obtained the shifts' values from the zero-zero point for four sources in three colours in five epochs. These shifts should be equal to the instrumental polarisation. It can be different for each camera, but should be the same for all sources in case of one camera. All the centres of circles and clumps for three colours and five epochs are presented in Fig. 1. There is a significant scatter of the centres coordinates in the first two epochs, that cover the time span from 56200 MJD to 56638 MJD. However, in the next epochs the system is getting more stable in terms of instrumental polarisation. The centres have similar coordinates for each source which means that they translate to the similar instrumental polarisation values. This way one is able to remove the instrumental contribution to the measured PD.

For each single observation we calculated and corrected Stokes parameters for the instrumental polarisation. In the next step we calculated the polarisation degree (PD) and the position angle (PA). For each MJD range between LT hardware changes the instrumental polarisation, PD factors and PA shifts as defined below:

$$\text{true PD} = \frac{\text{measured PD}}{\text{PD factor}} \quad (1)$$

and

$$\text{true PA} = \text{measured PA} + \text{ROTSKYPA} + \text{PA shift} \quad (2)$$

were calculated, where ROTSKYPA is the sky position angle of the image.

To derive the factors and shifts we scaled the measured PD

and PA with respect to published polarisation results of polarisation standard stars (Schmidt et al. 1992). In case of the data obtained with the blue camera we scale accordingly to the published averaged values for the B and V Johnson filters (see Table 2), i.e. to 6.523%, 5.5965% for BD +59 389 and BD +64 106, respectively. Similarly to the PD factors, the PA shifts for the blue camera were calculated with respect to the averaged values of the PA in the B and V Johnston filters, i.e. 98.115° and 96.89° for BD +59 389 and BD +64 106, respectively. For all data scaling we used averaged PD and PA factors of polarised standard stars, i.e. BD +59 389 and BD +64 106.

PD of zero-polarised standard stars calculated from shifted q and u values is shown in Fig. A8, A10 for G 191-B2B and HD 14069, respectively. The data from the red camera have much bigger scatter than the data from the blue camera in both cases. Obtained PD, according to the Eq. 1, and PA, according to Eq. 2, for two non-zero polarised standard stars are shown in Fig. A2, A5 and in Fig. A3, A6 for BD +59 389 and BD +64 106, respectively. In all cases it is clearly visible that the single data points in the last epoch have the smallest uncertainties, as well as they are less scattered in comparison to the other epochs. However, in case of BD 64+106 a quite strong variability also is present. We will be able to have stronger conclusions on the variability of this source from the data obtained after the latest hardware change.

5 RESULTS

The resulting PD factors and PA shifts for five consecutive epochs are gathered in Table 3. The average of averaged PD factors for all five epochs (56200–57400 MJD) is on the level of 0.802 for all three colours, while the averaged PA shift is around 76.297 degrees for the first three epochs (56200–56816 MJD), -41.024 degrees for the fourth epoch (56816–57200 MJD) and -74.886 degrees for the last epoch (57200–57400 MJD), again for all three colours.

As a test we also calculated the PA and PD with their errors for the case of 3 polarisers (0° , 45° , 135°) for the non-zero polarised source with the highest number of measurements, i.e. BD +59 389. The results show that using 8 polarisers reduces the errors of PA and PD by a mean factor of ~ 1.95 (with the maximum of 4.15) with respect to the case of 3 polarisers. Using more than 3 polarisers ensures diminishing of error estimations of the Stokes parameters and therefore PD and PA errors.

5.1 Time series

We also show normalised Stokes parameters (Q/I and U/I) of two unpolarised standard stars (G 191-B2B and HD 14069) as a function of time for five consecutive epochs (Fig. 2, 3, 4 and 5). For unpolarised standard, that by definition should not change as a function of time, one expects that Stokes parameters will be constant in time. From obtained plots one can read that this condition is the best fulfilled for G 191-B2B standard in the last epoch. HD 14069 shows some small, but significant trend in the fourth and fifth epoch, when the instrument was already well calibrated, especially in the case of the Stokes parameter U/I . For each standard, colour and epoch the linear model was fitted and the obtained a (slope) and b (intercept) parameters are gathered in the Table A1 and A2. These models can be used for the data calibration with respect to each epoch and colour. The most often observed unpolarised standard was G 191-B2B. It is the most stable over time as well, therefore we recommend this target as the best calibration target for other

Table 3. Polarisation PD factors as well as PA shift for five epochs. True PD is calculated as measured PD divided by PD factor, and true PA is calculated as PA shift added to measured PA.

MJD range	PD factor				PA shift [°]			
	blue	green	red	average	blue	green	red	average
56200 - 56315	0.816	0.919 ^a	0.808	0.812 ^b	75.322	74.049	76.635	75.335
56315 - 56638	0.801	0.806	0.806	0.804	77.107	76.358	77.115	76.86
56638 - 56816	0.818	0.82	0.777	0.805	77.18	76.434	76.47	76.695
56816 - 57200	0.817	0.828	0.802	0.816	-40.813	-41.38	-40.88	-41.024
57200 - 57400	0.754	0.763	0.808	0.775	-74.749	-75.314	-74.594	-74.886

^a There are not many data for the green camera during the first epoch, therefore the calculated PD factor is not meaningful.

^b This average is calculated only from the PD factors of the blue and the red cameras.

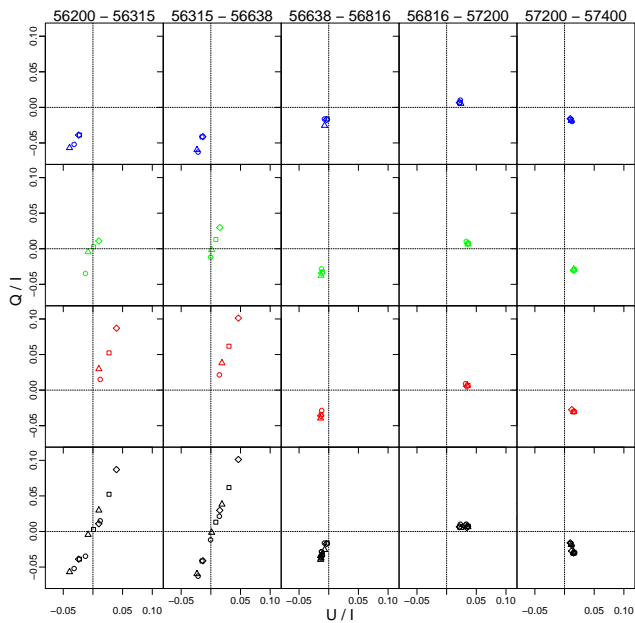


Figure 1. Weighted means of the normalised Stokes Q/I and U/I parameters for the unpolarised standard stars G 191-B2B (rhombus) and HD 14069 (square) and the centres of fitted circles for polarised standard stars BD +59 389 (circle) and BD +64 106 (triangle) as a function of time (five epochs in MJD). The bottom row contains all the points in all colours for all the standard stars for each epoch. The scatter is highest in the first two epochs (56200–56638 MJD) with the lowest value of scatter in the case of the blue camera and the biggest for the red one. In the last two epochs of 56816–57200 MJD and 57200–57400 MJD all the points are gathered around the same point which is very close to zero. This shows that the hardware changes improved the system significantly.

sources. In case of HD 14069 the small changes in U/I Stokes parameter, observed even in the last epoch, might be intrinsic and not instrumental.

For the fourth and fifth epochs the weighted means of Q/I and U/I along with the weighted standard deviations for G 191-B2B and HD 14069 were calculated and are gathered in Table 4 and 5.

5.2 Correlations

We also checked if there are any correlations between the observing conditions and derived values. There are no correlations of the PD or the PA with the Moon phase or the Moon distance from the source in any of the observed energy ranges. Pearson’s correlation

Table 4. Comparison of Q/I and U/I for two zero-polarised standard stars in the fourth epoch 56816–57200 MJD.

	G 191-B2B	HD 14069
Q/I_{blue}	0.00664 ± 0.00007	0.00631 ± 0.00006
Q/I_{green}	0.00722 ± 0.00017	0.00759 ± 0.0001
Q/I_{red}	0.00538 ± 0.00027	0.00667 ± 0.00014
U/I_{blue}	0.02152 ± 0.00007	0.02172 ± 0.00006
U/I_{green}	0.03561 ± 0.00017	0.03642 ± 0.0001
U/I_{red}	0.03396 ± 0.00027	0.03606 ± 0.00014

Table 5. Comparison of Q/I and U/I for two zero-polarised standard stars in the fifth epoch 57200–57400 MJD.

	G 191-B2B	HD 14069
Q/I_{blue}	-0.01593 ± 0.00009	-0.01683 ± 0.00003
Q/I_{green}	-0.03023 ± 0.00022	-0.03013 ± 0.00006
Q/I_{red}	-0.0274 ± 0.00037	-0.03071 ± 0.00008
U/I_{blue}	0.0097 ± 0.00009	0.01011 ± 0.00003
U/I_{green}	0.01519 ± 0.00022	0.01588 ± 0.00006
U/I_{red}	0.01207 ± 0.00037	0.01446 ± 0.00008

Table 6. The PD factors and the PA shifts in the fourth epoch 56816–57200 MJD.

colour	PD factor		PA shift [deg]	
	PD factor	PA shift [deg]	PD factor	PA shift [deg]
	BD +59 389		BD +64 106	
blue	0.767	-39.888	0.868	-41.738
green	0.768	-40.571	0.887	-42.189
red	0.75	-40.163	0.853	-41.596

Table 7. The PD factors and the PA shifts in the fifth epoch 57200–57400 MJD.

colour	PD factor		PA shift [deg]	
	PD factor	PA shift [deg]	PD factor	PA shift [deg]
	BD +59 389		BD +64 106	
blue	0.793	-76.055	0.715	-73.443
green	0.773	-76.424	0.754	-74.205
red	0.809	-75.552	0.807	-73.635

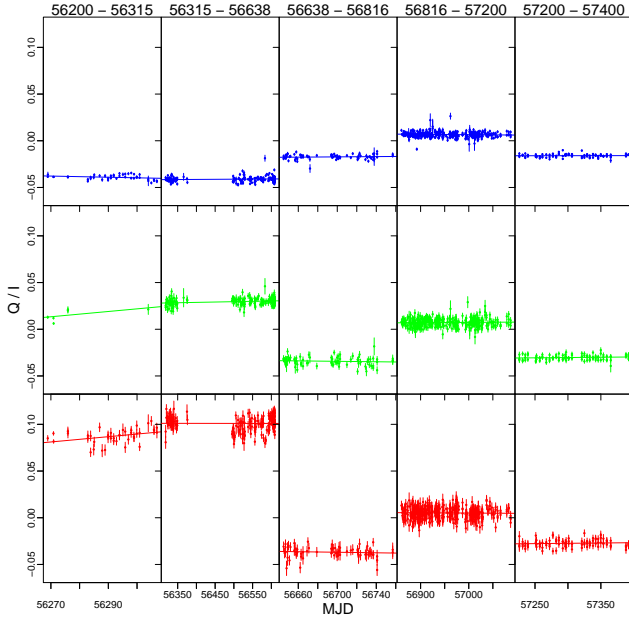


Figure 2. Normalised Stokes parameter Q/I for G 191-B2B as a function of time. There are not many data points from the green camera in the first epoch, therefore the Q/I dependence on time is not well constrained.

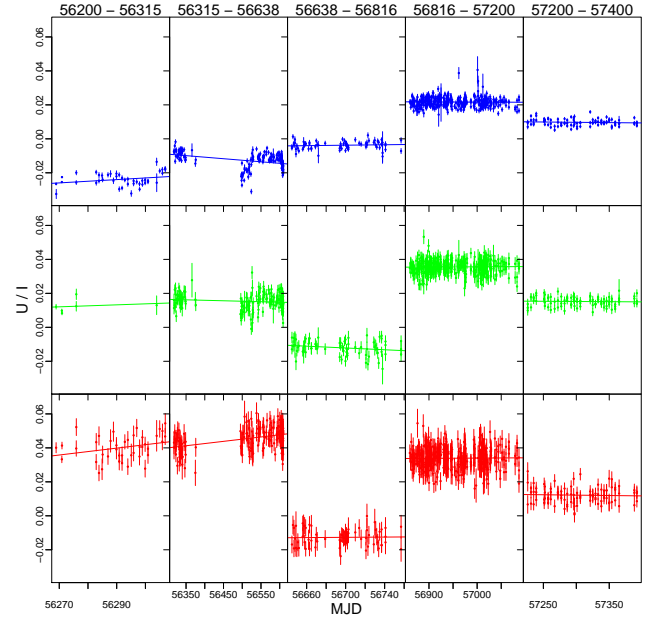


Figure 4. Normalised Stokes parameter U/I for G 191-B2B as a function of time. There are not many data points from the green camera in the first epoch, therefore the U/I dependence on time is not well constrained.

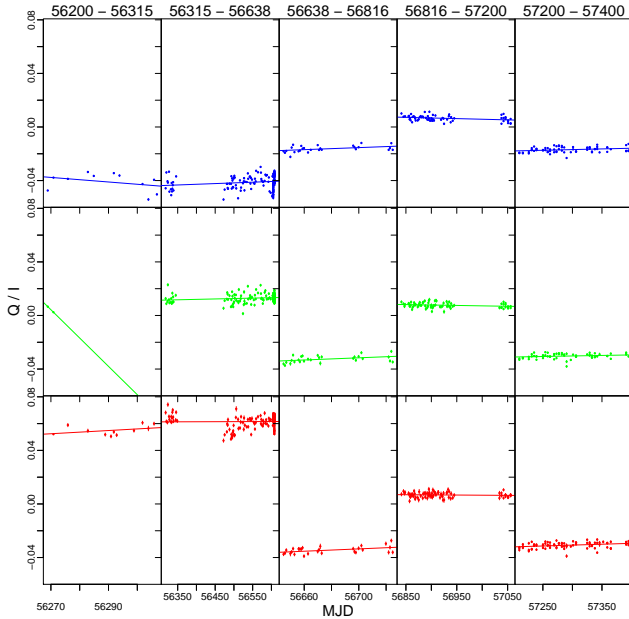


Figure 3. Normalised Stokes parameter Q/I for HD 14069 as a function of time. There are not many data points from the green camera in the first epoch, therefore the Q/I dependence on time is not well constrained.

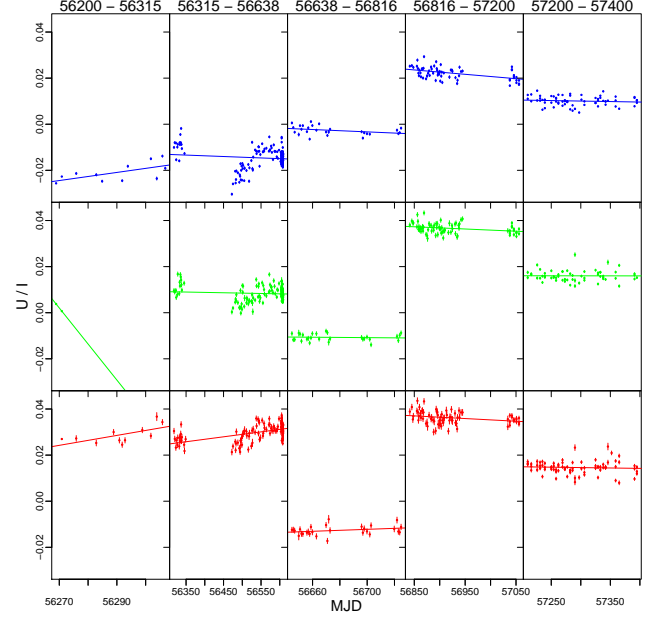


Figure 5. Normalised Stokes parameter U/I for HD 14069 as a function of time. There are not many data points from the green camera in the first epoch, therefore the U/I dependence on time is not well constrained.

coefficients for all sources in all energy ranges were $|r| < 0.1$. An example plot for the case of BD +59 389 is shown in Fig. 6.

However, there seem to be weak positive correlations between PD and seeing in BD +59 389. The larger the seeing, the larger the PD. The correlation coefficients are 0.47, 0.45 and 0.49 for blue, green and red cameras, respectively. In this case, the most likely explanation is that there is contamination from a nearby star which is 16 arcseconds away from the target. No significant correlations

were detected between PA and seeing. Figure 7 shows the PD as a function of seeing, measured as the FWHM of the radial light distribution of the star on the detector. BD +59 389 is the only star that shows this weak relationship. As a comparison, we also present data for BD +64 106 (lower panel of Fig. 7). No correlation is seen in this case.

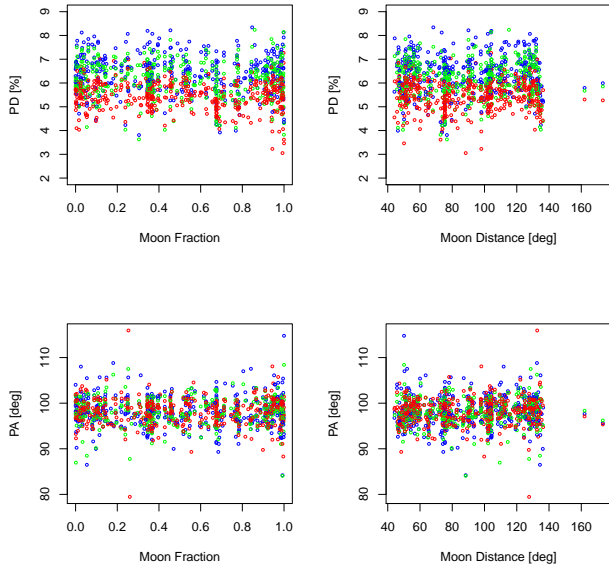


Figure 6. The PD and the PA of BD +59 389 as a function of the Moon fraction and the Moon distance from the source. There are no correlations between these values. Colours correspond to the data obtained with the respective cameras.

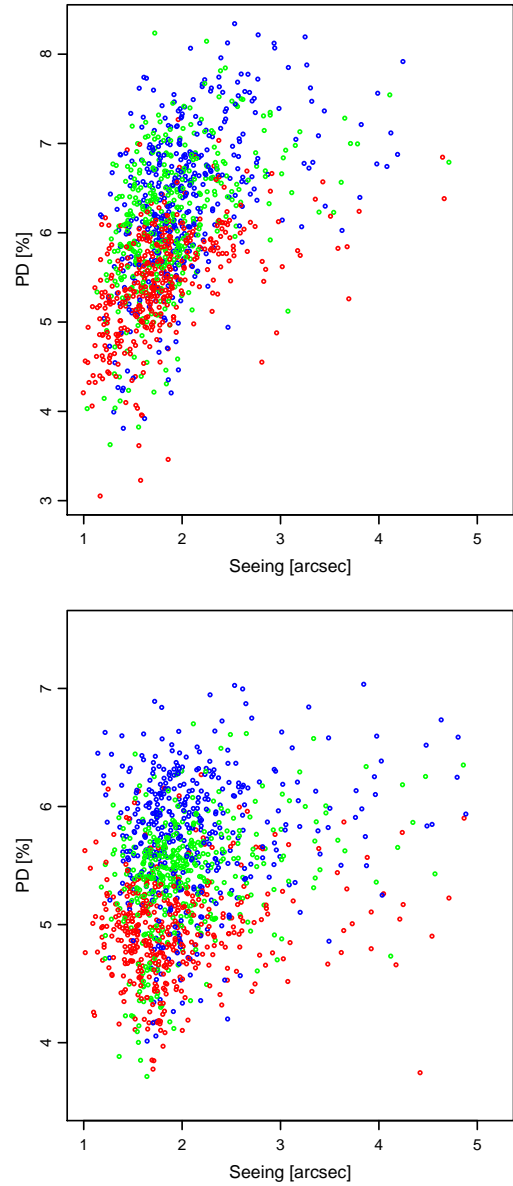


Figure 7. Dependence of the PD on the seeing for BD +59 389 (upper panel) and BD +64 106 (lower panel) in three camera colours for all available measurements. BD +59 389 is the only star on our list that shows a weak dependence of PD on seeing.

6 SUMMARY AND CONCLUSIONS

We have performed a long-term analysis of four polarimetric standard stars in order to calibrate the RINGO3 polarimeter operating at the Liverpool Telescope. Due to hardware changes, we divided the observations into five intervals. We have shown that the fifth interval provides the best calibrated results. Therefore we added five more standard stars to our analysis that were recently added and observed during the last epoch. Their measured polarisation degree as well as position angle are shown in Fig. 8 and Fig. 9, respectively. Resulting values as well as the catalogue values are gathered in Table 8. For BD +59 389 as well as for HD 14069 the gain was set to 100 before 57200 MJD and was changed to 20 after this date. Because both stars are brighter than 10th magnitude the read noise is not really important. Therefore it was basically the realuminization that improved the results in the last epoch and the EMGAIN setting did not have such a big influence.

The relationship between the RINGO3 values and the catalogue ones are shown in Fig. 10. For comparison the measured values of seven high polarisation standards (for details check the Table 1 of King et al. 2014) obtained with the Robopol polarimeter are shown. The relations between the RINGO3 measured values and the catalogued ones are summarised as follows:

$$\text{blue (B + V) : PD} = 0.7808 \cdot \text{PD}_{\text{cat}} + 0.1025,$$

$$\text{green (R) : PD} = 0.8364 \cdot \text{PD}_{\text{cat}} - 0.263,$$

$$\text{red (I) : PD} = 0.7475 \cdot \text{PD}_{\text{cat}} + 0.2061.$$

Table 8 gives the average and standard deviation of nine standard stars (seven polarisation standards and two zero-polarised standards) measured during the fifth epoch. Because the standard deviation measures the scattering around a mean value, the results from Table 8 can be used to check their stability with time.

Of the seven polarisation standard stars, BD +25 727 is the one showing the most stable results, with the lowest value of standard deviation in the polarisation degree with $\sim 0.2\%$, while HILT 960 displays the highest dispersion with 0.57% . Both zero-polarised standard stars display a rather constant polarisation degree over time. Although BD +59 389 appears to be less variable than BD +64 106, the former shows a correlation with the seeing conditions, which most likely results from the presence of a nearby star (Fig. 7). BD +64 106 appears to be more variable during the fifth epoch than it was before (see Fig. A5 and A6). More observations are needed to reveal if this star can be considered as a proper standard star. With respect to the polarisation angle, the scattering around the mean is $\lesssim 4^\circ$ for all sources.

The present work will be useful not only for RINGO3 users, but also as a reference for anyone performing polarimetric observations. With forthcoming big telescopes we are dramatically missing the faint polarimetric standard stars. Therefore, we need to not only verify which of known standard stars are stable ones, but there is also an urgent need to look for new and fainter ones. As for RINGO3 in particular, the observers would greatly benefit if the list of standard stars is extended to cover a larger range in polarisation degree, especially for polarisation degree between 2% and 4%, as can be seen in Fig. 10.

The results of our study should be applied to all polarimetric observations performed with RINGO3 between December 7th, 2012 — when the instrument was commissioned, and January 7th, 2016 — when the latest data presented in this publication were obtained. These dates correspond to 56268 MJD and 57394 MJD, re-

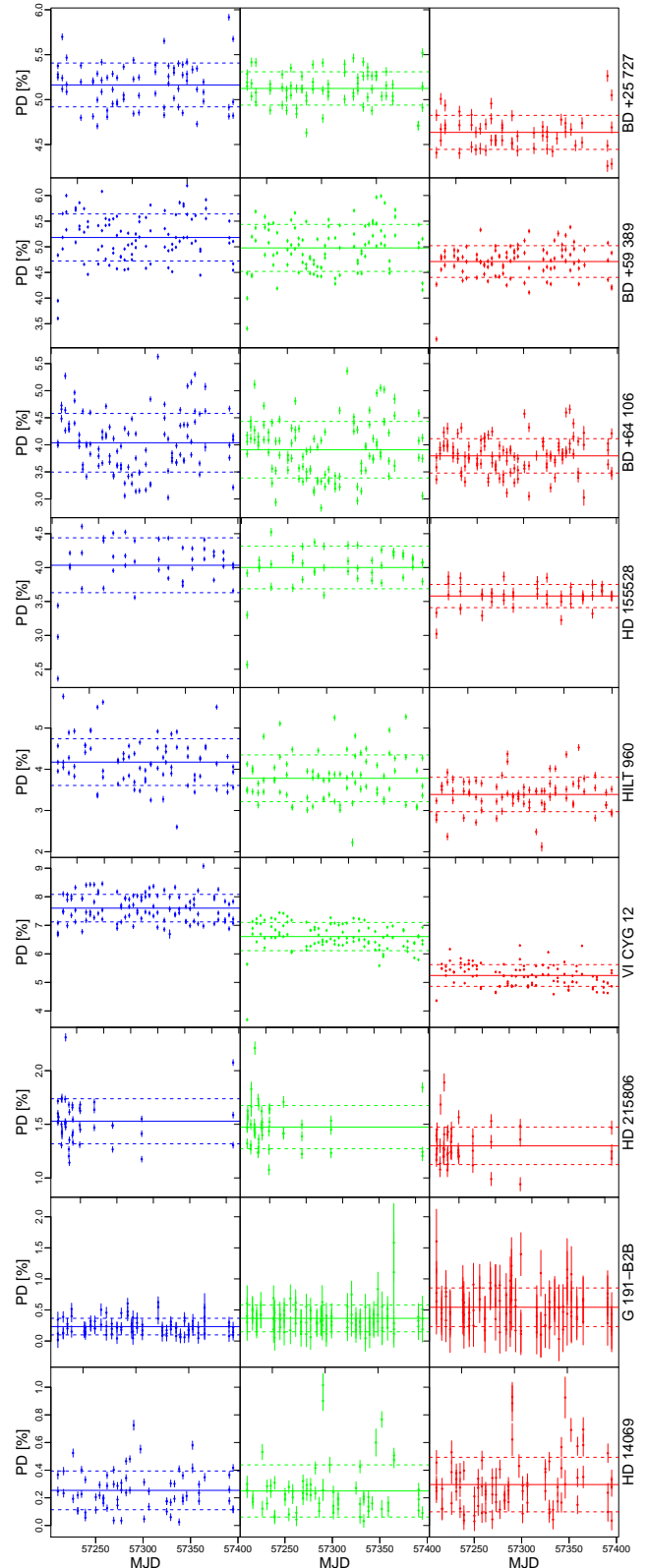


Figure 8. Measured PD not corrected for the PD factor of nine calibration standard stars in three colours in the last MJD epoch. Solid lines correspond to the mean values, while dotted lines to one standard deviation in each single panel (see also Table 8).

Table 8. The RINGO3 measured PD and PA values of polarised standard stars for the fifth epoch (57200–57400 MJD) together with their standard deviations (σ_{PD} , σ_{PA}) as well as with the respective catalogued values. Measured PD was not corrected for the PD factor, while the PA is corrected for the PA shift that is taken as an averaged value from Table 3 for the fifth epoch, i.e. -74.9 degrees. The catalogued values of PD, PA and magnitude for the blue camera are the mean values obtained for the B and V Johnston filters (see Table 2), whereas green and red cameras correspond to the R and I, respectively. The Count column gives the number of data points in each colour for each source. The value of EMGAIN setting during observations is also given.

Source	Camera	Count	PD [%]	σ_{PD} [%]	PD cat [%]	PA [deg]	σ_{PA} [deg]	PA cat [deg]	Brightness [mag]	EMGAIN
BD +25 727	blue	69	5.16	0.25	6.11	33.5	3.2	31.5	9.88	20
BD +25 727	green	68	5.12	0.19	6.29	33.8	2.5	31.0	9.11	20
BD +25 727	red	52	4.64	0.19	5.68	33.3	1.5	31.0	8.98	20
BD +59 389	blue	99	5.18	0.46	6.52	99.3	2.0	98.1	9.55	20
BD +59 389	green	101	4.98	0.46	6.43	99.7	1.8	98.1	8.49	20
BD +59 389	red	97	4.71	0.31	5.80	99.3	1.6	98.3	8.23	20
BD +64 106	blue	106	4.01	0.51	5.60	98.8	3.0	96.9	10.58	100
BD +64 106	green	107	3.89	0.51	5.15	99.3	2.8	96.7	9.90	100
BD +64 106	red	108	3.80	0.32	4.70	98.9	2.2	96.9	9.84	100
G 191-B2B	blue	93	0.23	0.13	0.08	–	–	–	11.55	100
G 191-B2B	green	93	0.35	0.18	–	–	–	–	11.82	100
G 191-B2B	red	92	0.54	0.31	–	–	–	–	11.45	100
HD 14069	blue	68	0.25	0.13	0.07	–	–	–	9.13	20
HD 14069	green	60	0.25	0.18	–	–	–	–	8.97	20
HD 14069	red	81	0.30	0.20	–	–	–	–	8.91	20
HD 155528	blue	45	4.03	0.40	4.80	93.4	2.8	91.9	9.83	20
HD 155528	green	45	4.00	0.31	–	94.6	2.0	–	9.32	20
HD 155528	red	44	3.58	0.17	–	94.4	2.1	–	9.16	20
HD 215806	blue	48	1.53	0.21	1.85	71.3	3.2	66.5	9.38	20
HD 215806	green	47	1.47	0.20	1.83	72.4	3.7	66.0	8.99	20
HD 215806	red	45	1.30	0.17	1.53	71.5	4.3	67.0	–	20
HILT 960	blue	80	4.17	0.57	5.69	56.0	4.2	54.9	10.96	100
HILT 960	green	80	3.78	0.57	5.21	55.5	3.7	54.5	9.84	100
HILT 960	red	80	3.39	0.42	4.46	55.0	3.7	54.0	9.49	100
VI CYG 12	blue	107	7.60	0.48	9.31	117.7	1.9	117.0	13.12	20
VI CYG 12	green	106	6.61	0.49	7.89	118.1	1.9	116.2	11.96	20
VI CYG 12	red	105	5.24	0.38	7.06	117.8	1.7	117.0	8.41	20

spectively. The data presented in this publication will be available as a catalogue at Vizier⁴ service, that will be updated periodically as the polarimetric standard stars are observed and new data are available.

⁴ <http://vizier.u-strasbg.fr/vizier/>

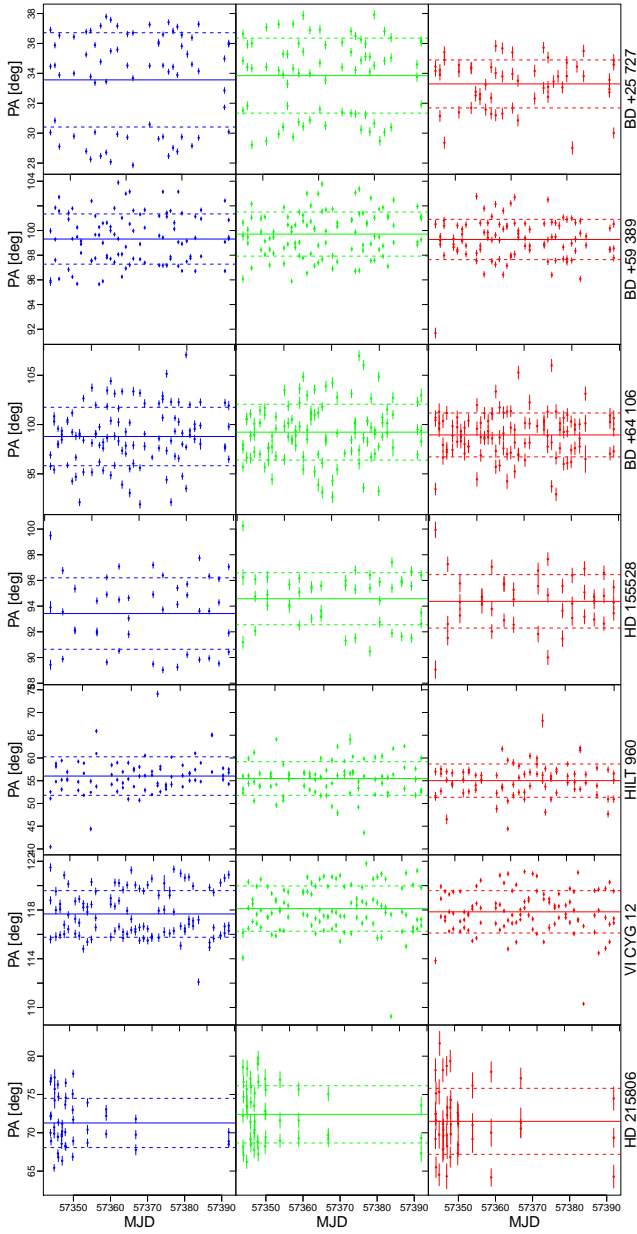


Figure 9. Measured PA of seven high polarisations standard stars in three colours in the last epoch (57200–57400 MJD). PA is corrected for the PA shift that is taken as an averaged value from Table 3 for the fifth epoch, i.e. -74.9 degrees. Solid lines correspond to the mean values, while dotted lines to one standard deviation in each single panel (see also Table 8).

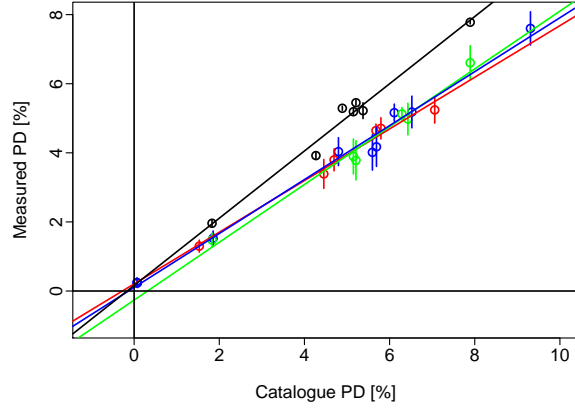


Figure 10. Measured PD as a function of catalogued PD for the blue, green and red cameras of the RINGO3 polarimeter (colour coded). The colours of the RINGO3 blue, green and red cameras approximately correspond to the B+V, R and I, respectively. For comparison the RoboPol polarimeter data are also shown (black points and black solid line, after Table 1 of King et al. (2014)). RoboPol polarimeter works in the Johnson R-band.

ACKNOWLEDGEMENTS

We are grateful to the anonymous referee whose suggestions helped us to improve our paper significantly. We are also very grateful to Frans Snik for his valuable comments and discussion as well as to Hervé Lamy for chairing the COST Action MP1104 and all the support and possibilities of extending our knowledge on polarisation that we got during this action. We are grateful to Helen Jermak for technical assistance. This work has been supported by Polish National Science Centre grant DEC-2011/03/D/ST9/00656 (AS, KK, MŻ). This research was partly supported by the EU COST Action MP1104 "Polarization as a tool to study the solar system and beyond" within STSM projects: COST-STSM-MP1104-14064, COST-STSM-MP1104-16823 COST-STSM-MP1104-14070 and COST-STSM-MP1104-16821. Data analysis and figures were partly prepared using R (R Core Team 2013). The Liverpool Telescope is operated on the island of La Palma by Liverpool John Moores University in the Spanish Observatorio del Roque de los Muchachos of the Instituto de Astrofísica de Canarias with financial support from the UK Science and Technology Facilities Council.

REFERENCES

- Abdo A. A., Ackermann M., Ajello M., Axelsson M., Baldini L., Ballet J., Barbiellini G., Bastieri D., Baughman B. M., Bechtol K., et al. 2010, *Nature*, 463, 919
- Arnold D. M., Steele I. A., Bates S. D., Mottram C. J., Smith R. J., 2012, in *Society of Photo-Optical Instrumentation Engineers (SPIE) Conference Series Vol. 8446 of Society of Photo-Optical Instrumentation Engineers (SPIE) Conference Series, RINGO3: a multi-colour fast response polarimeter*. p. 2
- Bertin E., Arnouts S., 1996, *A&AS*, 117, 393
- Graham J. R., Kalas P. G., Matthews B. C., 2007, *ApJ*, 654, 595
- Hansen J. E., Hovenier J. W., 1974, *Journal of Atmospheric Sciences*, 31, 1137
- King O. G., Blinov D., Ramaprakash A. N., Myserlis I., et al. A., 2014, *MNRAS*, 442, 1706
- Moran P., Shearer A., Mignani R. P., Słowikowska A., De Luca A., Gouiffès C., Laurent P., 2013, *MNRAS*, 433, 2564
- Mundell C. G., Kopač D., Arnold D. M., Steele I. A., Gomboc A., Kobayashi S., Harrison R. M., Smith R. J., Guidorzi C., Virgili F. J., Melandri A., Japelj J., 2013, *Nature*, 504, 119
- R Core Team 2013, *R: A Language and Environment for Statistical Computing*. R Foundation for Statistical Computing, Vienna, Austria
- Schmidt G. D., Elston R., Lupie O. L., 1992, *AJ*, 104, 1563
- Słowikowska A., Kanbach G., Kramer M., Stefanescu A., 2009, *MNRAS*, 397, 103
- Sparks W. B., Axon D. J., 1999, *PASP*, 111, 1298
- Steele I. A., Smith R. J., Rees P. C., et al., 2004, in *Oschmann Jr. J. M., ed., Ground-based Telescopes Vol. 5489 of Society of Photo-Optical Instrumentation Engineers (SPIE) Conference Series, The Liverpool Telescope: performance and first results*. pp 679–692
- Turnshek D. A., Bohlin R. C., Williamson II R. L., Lupie O. L., Koornneef J., Morgan D. H., 1990, *AJ*, 99, 1243
- Whittet D. C. B., Martin P. G., Hough J. H., Rouse M. F., Bailey J. A., Axon D. J., 1992, *ApJ*, 386, 562

APPENDIX A: APPENDIX

A1 Polarisation calculations and error propagation

A1.1 Sparks & Axon

Stokes from Sparks & Axon: $I_i, Q_i, U_i, \sigma_i, \sigma_{Q_i}$ and σ_{U_i} , where i denotes single observation, i.e. intensity measured in 8 polariser positions. Let us define $q_i = Q_i/I_i$ and $u_i = U_i/I_i$ with respective errors $\sigma_{q_i} = \sqrt{(\frac{1}{I_i}\sigma_{Q_i})^2 + (-\frac{Q_i}{I_i^2}\sigma_i)^2}$ and $\sigma_{u_i} = \sqrt{(\frac{1}{I_i}\sigma_{U_i})^2 + (-\frac{U_i}{I_i^2}\sigma_i)^2}$.

A1.2 Shifts

For non-polarised standard stars $q_i^s = q_i - \bar{q}$, $u_i^s = u_i - \bar{u}$ where means are weighted means calculated from observations from the same MJD range between LT hardware changes:

$$\bar{q} = \frac{\sum_i q_i / \sigma_{q_i}^2}{\sum_i 1 / \sigma_{q_i}^2}, \bar{u} = \frac{\sum_i u_i / \sigma_{u_i}^2}{\sum_i 1 / \sigma_{u_i}^2}$$

$$\sigma_{\bar{q}} = \sqrt{\frac{1}{\sum_i 1 / \sigma_{q_i}^2}}, \sigma_{\bar{u}} = \sqrt{\frac{1}{\sum_i 1 / \sigma_{u_i}^2}}$$

Shifted q_i^s and u_i^s with their corresponding errors:

$$q_i^s = q_i - \bar{q}, u_i^s = u_i - \bar{u}$$

$$\sigma_{q_i^s} = \sqrt{\sigma_{q_i}^2 + \sigma_{\bar{q}}^2}, \sigma_{u_i^s} = \sqrt{\sigma_{u_i}^2 + \sigma_{\bar{u}}^2}$$

Instrumental polarisation:

$$\text{IP} = \sqrt{\bar{q}^2 + \bar{u}^2}$$

$$\sigma_{\text{IP}} = \sqrt{\frac{\bar{q}^2}{\bar{q}^2 + \bar{u}^2} \sigma_{\bar{q}}^2 + \frac{\bar{u}^2}{\bar{q}^2 + \bar{u}^2} \sigma_{\bar{u}}^2}$$

Polarisation degree (PD_{*i*}) calculated from q_i^s and u_i^s :

$$\text{PD}_i = \sqrt{(q_i^s)^2 + (u_i^s)^2} \cdot 100\%$$

$$\sigma_{\text{PD}_i} = \sqrt{\frac{(q_i^s)^2}{(q_i^s)^2 + (u_i^s)^2} \sigma_{q_i^s}^2 + \frac{(u_i^s)^2}{(q_i^s)^2 + (u_i^s)^2} \sigma_{u_i^s}^2} \cdot 100\%$$

Polarisation angle (PA_{*i*}) calculated from q_i^s and u_i^s :

$$\text{PA}_i = \frac{1}{2} \arctan\left(\frac{u_i^s}{q_i^s}\right) \cdot \frac{180^\circ}{\pi}$$

$$\sigma_{\text{PA}_i} = \sqrt{\left(\frac{1}{2q_i^s(1 + (u_i^s)^2/(q_i^s)^2)}\right)^2 \sigma_{u_i^s}^2 + \left(-\frac{u_i^s}{2((q_i^s)^2 + (u_i^s)^2)}\right)^2 \sigma_{q_i^s}^2} \cdot \frac{180^\circ}{\pi}$$

Table A1. Linear fits of Q/I as a function of MJD in the form of $Q/I = a \cdot \text{MJD} + b$. There are not enough data points in case of HD 14069 in green colour in the first epoch.

MJD range	Source	blue		Q/I green		red	
		a [10 ⁻⁵]	b	a [10 ⁻⁵]	b	a [10 ⁻⁵]	b
56200 - 56315	G 191-B2B	-6.22588 ± 3.7067	3.4655 ± 2.08656	28.22669 ± 18.88837	-15.86979 ± 10.62995	28.26401 ± 11.61088	-15.82304 ± 6.53599
	HD 14069	-17.02482 ± 15.08858	9.54221 ± 8.49333	—	—	12.02995 ± 9.76139	-6.71683 ± 5.49481
56315 - 56638	G 191-B2B	0.24016 ± 0.19987	-0.17684 ± 0.11299	0.76741 ± 0.24999	-0.40406 ± 0.14132	-0.04385 ± 0.52521	0.12577 ± 0.29691
	HD 14069	1.04026 ± 0.49436	-0.62949 ± 0.27956	0.62723 ± 0.31245	-0.34174 ± 0.17669	0.08544 ± 0.46375	0.0132 ± 0.26224
56638 - 56816	G 191-B2B	0.72573 ± 0.93509	-0.42874 ± 0.53014	-1.16802 ± 1.69196	0.62793 ± 0.95924	-1.45806 ± 2.20054	0.78977 ± 1.24758
	HD 14069	3.82252 ± 1.55795	-2.18277 ± 0.88297	4.06072 ± 1.70524	-2.33404 ± 0.96647	4.34963 ± 1.62387	-2.49979 ± 0.92038
56816 - 57200	G 191-B2B	-0.39898 ± 0.25109	0.23392 ± 0.143	0.30698 ± 0.38481	-0.16762 ± 0.21916	-0.29263 ± 0.54787	0.17182 ± 0.31202
	HD 14069	-0.93964 ± 0.34431	0.54138 ± 0.19601	-0.63593 ± 0.33158	0.36966 ± 0.18875	-0.2452 ± 0.34043	0.1463 ± 0.19379
57200 - 57400	G 191-B2B	0.07742 ± 0.40258	-0.06033 ± 0.23069	0.6248 ± 0.62988	-0.38828 ± 0.36095	0.6673 ± 0.89742	-0.40973 ± 0.51425
	HD 14069	1.01692 ± 0.4484	-0.59958 ± 0.2569	0.78509 ± 0.48007	-0.48009 ± 0.27504	1.32394 ± 0.45557	-0.78934 ± 0.261

Table A2. Linear fits of U/I as a function of MJD in the form of $U/I = a \cdot \text{MJD} + b$. There are not enough data points in case of HD 14069 in green colour in the first epoch.

MJD range	Source	blue		U/I green		red	
		a [10 ⁻⁵]	b	a [10 ⁻⁵]	b	a [10 ⁻⁵]	b
56200 - 56315	G 191-B2B	9.74502 ± 5.54679	-5.50947 ± 3.12238	5.868 ± 14.29402	-3.28986 ± 8.04435	20.2827 ± 11.30336	-11.37728 ± 6.36288
	HD 14069	17.61409 ± 7.36892	-9.93589 ± 4.14795	—	—	21.55379 ± 8.76519	-12.10408 ± 4.93404
56315 - 56638	G 191-B2B	-1.80915 ± 0.28135	1.00956 ± 0.15905	-0.55277 ± 0.31311	0.32767 ± 0.177	2.58749 ± 0.39251	-1.4168 ± 0.22189
	HD 14069	-0.61845 ± 0.44185	0.33511 ± 0.24987	-0.31433 ± 0.32345	0.1861 ± 0.18291	2.14438 ± 0.28758	-1.18256 ± 0.16262
56638 - 56816	G 191-B2B	0.66244 ± 0.82917	-0.37935 ± 0.47009	-2.64107 ± 1.50799	1.48532 ± 0.85494	0.38329 ± 1.89424	-0.23 ± 1.07392
	HD 14069	-2.55777 ± 1.32826	1.44693 ± 0.75279	-0.46136 ± 1.10551	0.25078 ± 0.62656	2.13545 ± 1.34432	-1.22301 ± 0.76193
56816 - 57200	G 191-B2B	-0.09761 ± 0.25007	0.07728 ± 0.14243	0.13613 ± 0.34261	-0.04197 ± 0.19513	0.16111 ± 0.55307	-0.05785 ± 0.31498
	HD 14069	-1.90078 ± 0.41329	1.10415 ± 0.23527	-0.9641 ± 0.38435	0.58538 ± 0.21879	-1.1615 ± 0.44841	0.69734 ± 0.25526
57200 - 57400	G 191-B2B	-0.36752 ± 0.4402	0.22032 ± 0.25225	-0.23515 ± 0.61656	0.14996 ± 0.35331	-0.44733 ± 1.09518	0.26849 ± 0.62757
	HD 14069	-0.42762 ± 0.47583	0.25508 ± 0.27262	-0.02817 ± 0.62404	0.03215 ± 0.35752	-0.34508 ± 0.59687	0.21232 ± 0.34196

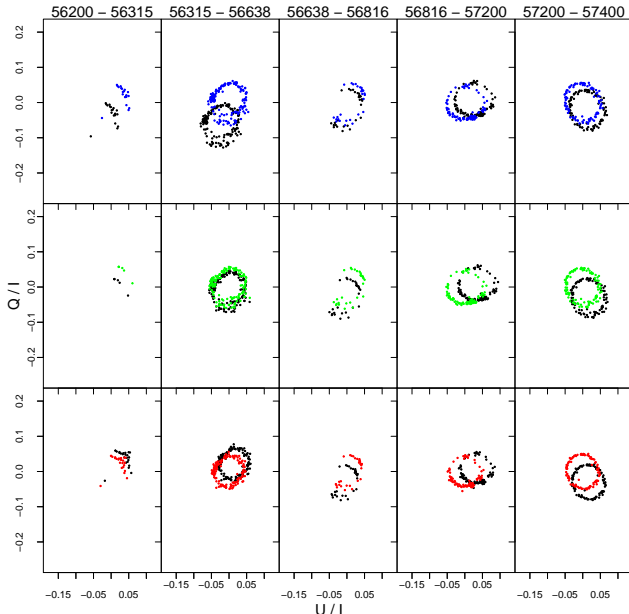


Figure A1. Normalised Q/I , U/I diagram of BD +59 389 for five time span ranges for the blue, green and red cameras from the top to the bottom, respectively. Black points denote measurements before shifts while colour ones are shifted to (0, 0) origin and correspond to the respective camera. For polarised source the points follow a circle because of the Alt-Az mount of the telescope.

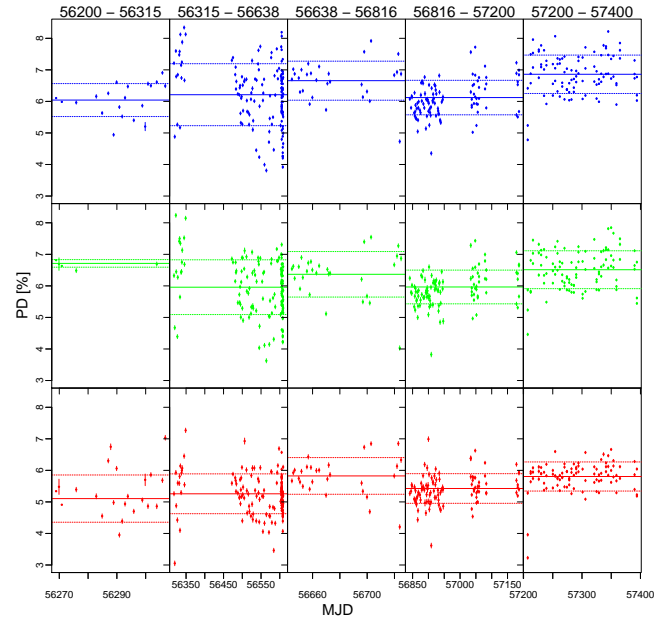


Figure A2. Resulting PD of BD +59 389 for five time span ranges for the blue, green and red cameras from the top to the bottom, respectively. Solid lines correspond to the mean values, while dotted lines to one standard deviation in each single panel. There are not many data points from the green camera in the first epoch, therefore the PD is not well constrained.

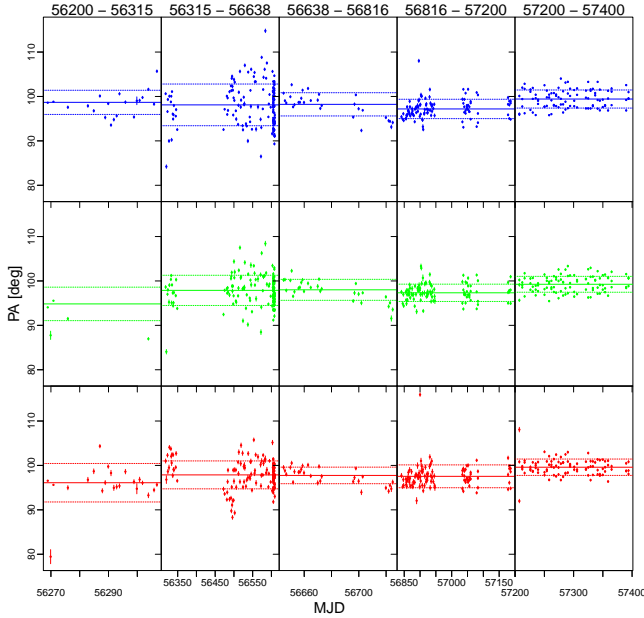


Figure A3. Resulting PA of BD +59 389 for five time span ranges for the blue, green and red cameras from the top to the bottom, respectively. Solid lines correspond to the mean values, while dotted lines to one standard deviation in each single panel. There are not many data points from the green camera in the first epoch, therefore the PA is not well constrained.

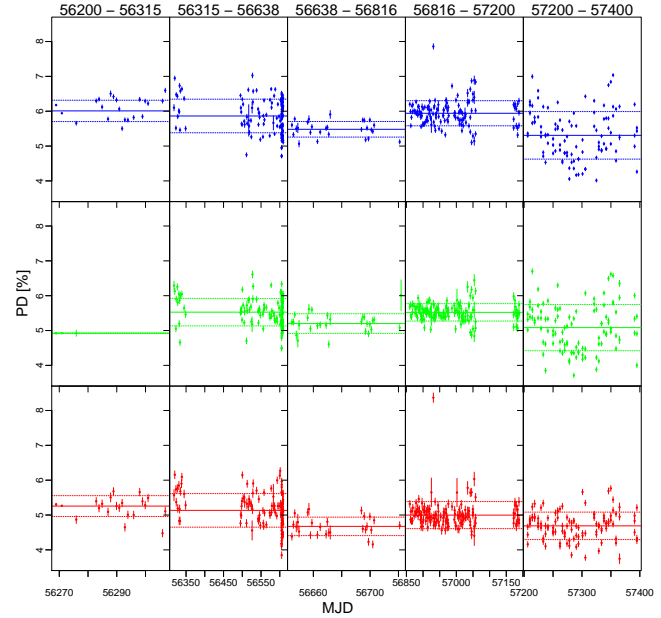


Figure A5. Resulting PD of BD +64 106 for five time span ranges for the blue, green and red cameras from the top to the bottom, respectively. Solid lines correspond to the mean values, while dotted lines to one standard deviation in each single panel. There are not many data points from the green camera in the first epoch, therefore the PD is not well constrained.

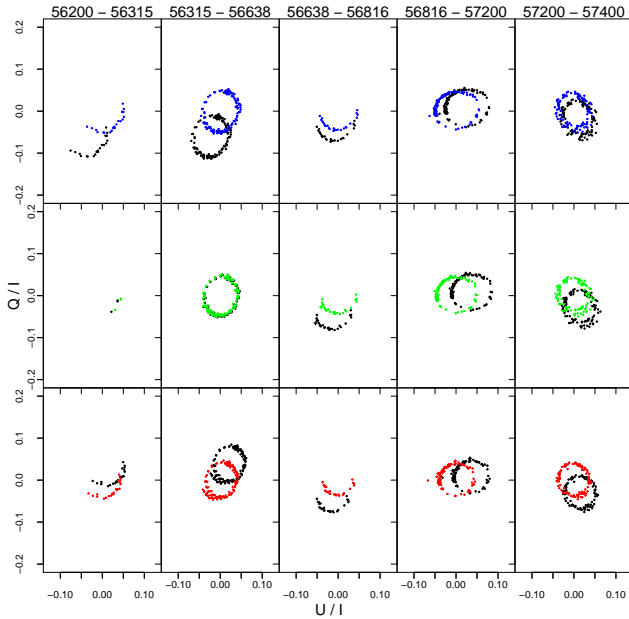


Figure A4. Normalised Q/I, U/I diagram of BD +64 106 for five time span ranges for the blue, green and red cameras from the top to the bottom, respectively. Black points denote measurements before shifts while colour ones are shifted to (0, 0) origin and correspond to the respective camera. For polarised source the points follow a circle because of the Alt-Az mount of the telescope.

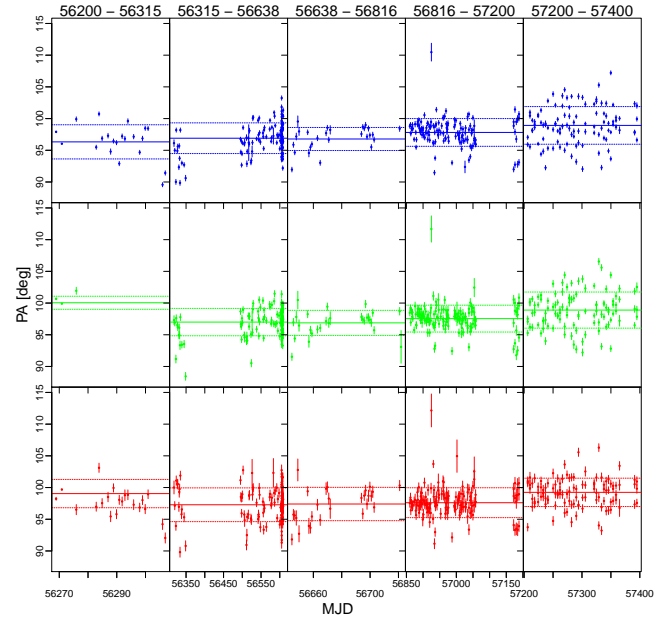


Figure A6. Resulting PA of BD +64 106 for five time span ranges for the blue, green and red cameras from the top to the bottom, respectively. Solid lines correspond to the mean values, while dotted lines to one standard deviation in each single panel. There are not many data points from the green camera in the first epoch, therefore the PA is not well constrained.

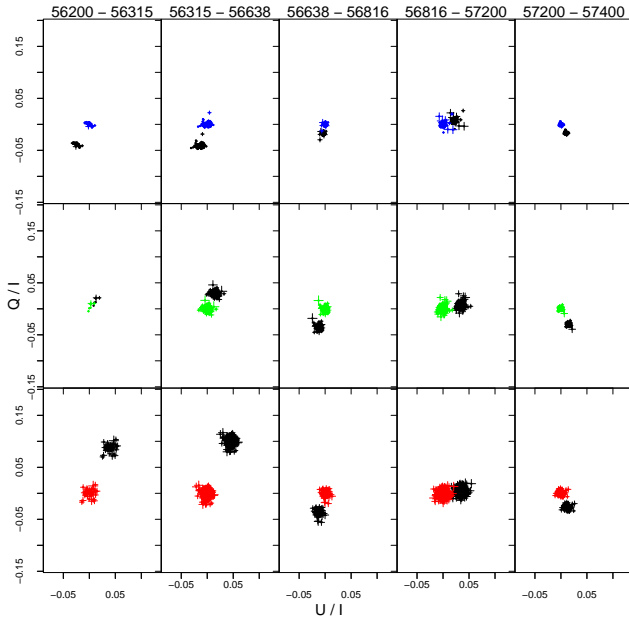


Figure A7. Normalised Q/I , U/I diagram of G 191-B2B for five time span ranges for the blue, green and red cameras from the top to the bottom, respectively. Black points denote measurements before shifts while colour ones are shifted to $(0, 0)$ origin and correspond to the respective camera.

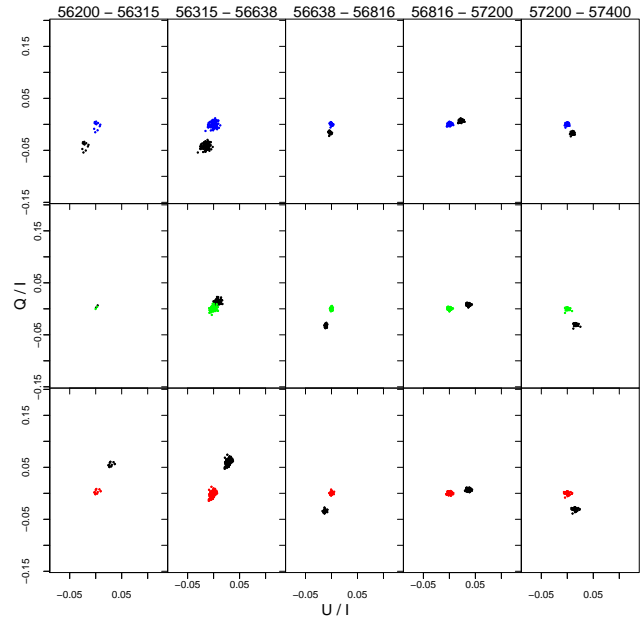


Figure A9. Normalised Q/I , U/I diagram of HD 14069 for five time span ranges for the blue, green and red cameras from the top to the bottom, respectively. Black points denote measurements before shifts while colour ones are shifted to $(0, 0)$ origin and correspond to the respective camera.

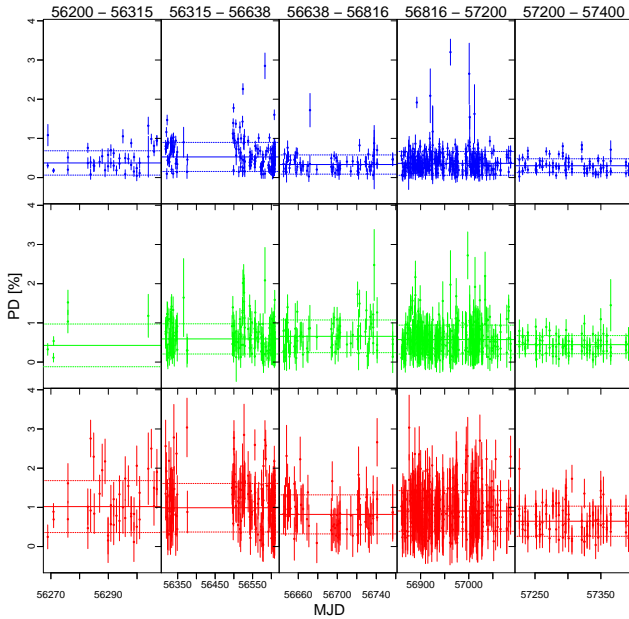


Figure A8. Resulting PD of G 191-B2B for five time span ranges for the blue, green and red cameras from the top to the bottom, respectively. Solid lines correspond to the mean values, while dotted lines to one standard deviation in each single panel.

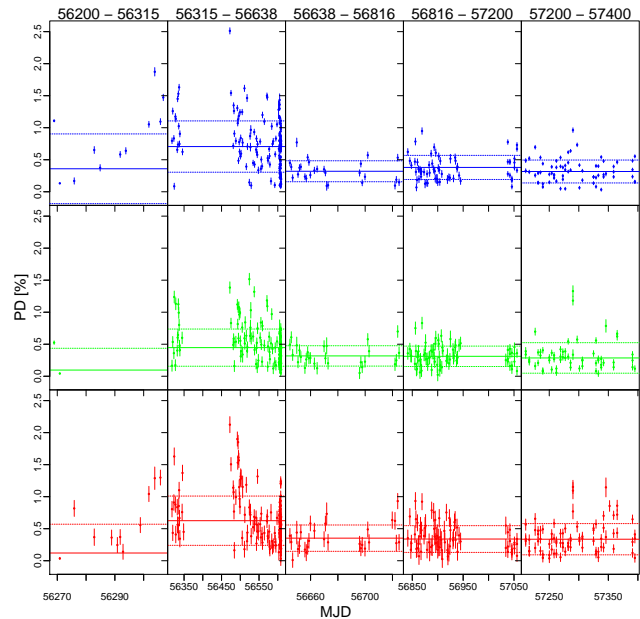


Figure A10. Resulting PD of HD 14069 for five time span ranges for the blue, green and red cameras from the top to the bottom, respectively. Solid lines correspond to the mean values, while dotted lines to one standard deviation in each single panel.